

Topological and topological-electronic correlations in amorphous silicon

Yue Pan,^{*} Mingliang Zhang,[†] and D. A. Drabold[‡]

Department of Physics and Astronomy, Ohio University, Athens, OH 45701

(Dated: February 7, 2022)

In this paper, we study several structural models of amorphous silicon, and discuss structural and electronic features common to all. We note spatial correlations between short bonds, and similar correlations between long bonds. Such effects persist under a first principles relaxation of the system and at finite temperature. Next we explore the nature of the band tail states and find the states to possess a filamentary structure. We detail correlations between local geometry and the band tails.

PACS numbers: 61.43.Dq, 71.23.An, 71.23.Cq

I. INTRODUCTION

The nature of three-dimensional space-filling disordered networks is salient to a variety of topics in scientific research. Despite work in recent decades, a number of puzzles remain both about the structure and connectivity of such networks. Also, important quantities *derived from* such structures (such as electronic or vibrational states) are quite incompletely understood, though their characteristics are ultimately derivative from the underlying structure. In this paper, we systematically consider a collection of (largely) tetrahedral continuous random networks of amorphous Si, and despite the fact that several of these are quite “standard”, we detect and report novel features of their connectivity and electronic structure.

The character of the tail states in disordered semiconductors is a problem of importance with a history dating back at least to the sixties. It has long been understood that band tail states in amorphous semiconductors arise from strains in the network sufficient to push states past the band edges into the gap. Such tails decay exponentially into the gap: this feature, nearly universal to disordered semiconductors, is called Urbach tailing.¹ Clever photoemission experiments allow the separate observation of the valence and conduction tails and even the temperature dependence of the tailing². Several theories have been presented to explain the Urbach tails, most recently by Cohen and coworkers.^{3,4}

Beside band tailing and the detailed structure of the networks we study, our work is related to the general problem of the topology of space-filling networks. For example, work on the cuprates^{5,6} provides clear, albeit circumstantial evidence for the existence of percolating filamentary networks, and is seen in STM measurements⁷ (presumably two-D projections of the three-D filamentary network). Filamentary paths are also believed to exist in fast ion conducting glasses with larger than average free volume⁸ regions providing pathways for ion transport (see for example Fig. 3 in Ref.⁸). Farther afield, results akin to ours (the percolation of short bonds) can be inferred in protein binding in a yeast⁹.

This paper has two immediate aims. First, consideration of several models reveals certain persistent geometri-

cal features, notably strong self-correlations between configurations involving short bonds and analogous correlations involving long bonds. To the extent that these correlations exist in various structural models and survive *ab initio* thermal molecular dynamics (MD) simulations, it seems worthwhile to point these out. The second aim is to discuss general features of the band tail states in a-Si. Resonant cluster proliferation of tail and gap states is observed¹⁰, and filamentary connections between localization centers. In agreement with earlier reports^{11,12}, we observe a robust tendency for valence (conduction) tail states to be associated with short (long) bonds. Unlike our earlier report¹¹, we did detect analogous features for the bond angle distribution, where we see that smaller (larger) bond angles are correlated with valence (conduction) tails.

These general observations about the tail states in a-Si are relevant to calculations of transport, since it is presumably just these states through which carriers hop, as we discuss in detail elsewhere¹³.

II. CONSTRAINTS ON THEORY

A. Model characteristics and nomenclature

Even in good quality unhydrogenated material, mid-gap defects are fairly rare, at most a few sites per thousand¹⁴. At a practical level this means that ideal models of tractable size (up to several thousand atoms) can contain zero to a few defects producing mid-gap states. The Wooten-Weaire-Winer (WWW)¹⁵ method is the “gold standard” for forming such realistic models, and several of the models we discuss depend upon WWW at least as a starting point. For completeness, and in particular to ascertain the extent to which our observations might tend to be WWW artifacts, we have repeated the calculations for other models as well. We summarize some salient features of the models in Table I.

#	Author	NOA	Type	$\Delta\theta/\Delta\cos\theta$	Δb	De%
M ₁	DTW ¹⁹	512	WWW	20.1°/0.33	0.08	0.0
M ₂	DTW ¹⁹	4096	WWW	19.1°/0.31	0.19	0.2
M ₃	Feldman ²⁰	1000	WWW	18.4°/0.30	0.08	4.0
M ₄	Mousseau ¹⁶	4000	ART ¹⁶	17.8°/0.30	0.11	4.0
M ₅	Nakhmanson ¹⁷	1000	PC	N/A	N/A	0.0
M ₆	Biswas ¹⁸	216	RMC ¹⁸	22.3°/0.37	0.30	12.5
M ₇	Biswas ¹⁸	500	RMC ¹⁸	22.5°/0.37	0.24	12
M ₈	Mousseau	64	WWW	20.7°/0.34	0.11	0.0
M ₉	DTW ¹⁹	216	WWW	24.5°/0.40	0.30	0.0

TABLE 1. Models and basic information. NOA stands for “Number of atoms”; De% stands for “defects percentage”; $\Delta\theta/\Delta\cos\theta$ stands for the width of bond-angle $\theta/\cos\theta$ distribution; Δb stands for the width of bond-length distribution; WWW stands for Wooten-Weaire-Winer modeling scheme¹⁵; ART stands for activation-relaxation technique¹⁶; PC stands for “paracrystalline”; RMC stands for Reverse Monte-Carlo modeling scheme¹⁸.

M₁, M₂, M₃, M₈ and M₉ all derived originally from WWW¹⁵ modeling scheme. M₁, M₂ and M₉ were developed by B. R. Djordjevic, M. F. Thorpe, F. Wooten¹⁹; M₃ was developed by Feldman and M₈ by N. Mousseau. M₄ was made via activation-relaxation technique¹⁶. M₅ and M₆ are Reverse-Monte-Carlo¹⁸ models. Model M₁ to M₄ and M₆ to M₉ are continuous random network (CRN) models. Beside CRN models, we include model M₅, a paracrystalline model (CRN with crystalline inclusion). In particular for M₅, 211 crystalline silicon atoms are embedded.

Excepting M₅, all the models that we have studied here have normally distributed bond lengths and cosines of bond angles. For the large WWW models the similarity to the normal distribution is quite striking²¹. Here we report the bond length and bond angle distributions for these models in Fig. 1. Model M₁ and M₄ show nearly perfect Gaussian fits, while model M₇, (a 500-atom model), is fairly Gaussian, with statistical noise. The other models exhibit similar traits. Dong and Drabold²¹ have attempted to correlate these normally-distributed quantities to Urbach tailing.

Model M₁, M₅, M₈ and M₉ are defect free. In the other models, there are coordination defects, ranging from 0.2% to 12.5%, including both dangling bonds and five-fold “floating” bonds. The pair correlation functions of these models are all similar, accurately reflecting the experimental function. As usual with a-Si, this is a reminder that the information in the pair-correlation function alone is very insufficient to specify coordinates.

B. Local inter-bond correlations

Our inspection of the topology of the models reveals that there is a tendency for short bonds to be linked to other short bonds and long bonds to be linked to other long bonds. In particular, this leads to 1) a tendency to spatial separation of the shortest and the longest bonds

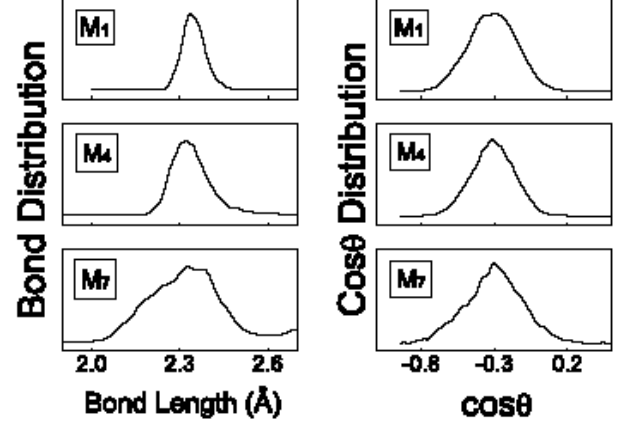


FIG. 1: Bond length distribution for model M₁, M₄ and M₇ (left column); Cosine bond angle distribution for model M₁, M₄ and M₇ (right column).

in the system; 2) a tendency to build up chain and ring like structures among extreme bonds. Selected fractions of shortest and longest bonds of model M₁ are extracted from the models and displayed in Fig. 2. The correlation is clearly visible, especially in Fig. 2c-f. Interpenetrating filamentary structures appear to percolate through space for a sufficiently large cutoff in the fractions of bonds displayed. For comparison, the 4% shortest and 4% longest bonds of model M₂ - M₇ are shown in Fig. 3. To some extent, the self-correlations of short and long bonds are visible in every model shown, suggesting that such bond correlations are not an artifact of a particular model or modeling scheme.

To explore our observation more quantitatively, we computed bond-bond correlation functions for the shortest and longest bonds:

$$\beta(r) = \frac{V}{4\pi r^2 N_1 N_2} \sum_{n_1=1}^{N_1} \sum_{n_2 \neq n_1}^{N_2} \delta(r_{n_1 n_2} - r) \quad (1)$$

where N_1 , N_2 are the number of short or long bonds as needed; n_1 and n_2 count over these particular bonds; $r_{n_1 n_2}$ is the distance between the bond centers of bond n_1 and bond n_2 ; V is the volume of the unit cell. The 4% shortest and 4% longest bonds are taken for model M₁ and the corresponding bond-bond correlation functions for (1) $N_1 = 4\%$ shortest, $N_2 = 4\%$ longest; (2) $N_1 = 4\%$ shortest, $N_2 = 4\%$ shortest; (3) $N_1 = 4\%$ longest, $N_2 = 4\%$ longest are plotted in Fig. 4. The first peaks of the correlations of the same-type bonds (grey and dotted lines) appear to be much stronger than the correlation between the different-type bonds (solid black line). The second and even the third peaks maintain this feature, and after 6.0 Å, this correlation wanes. This con-

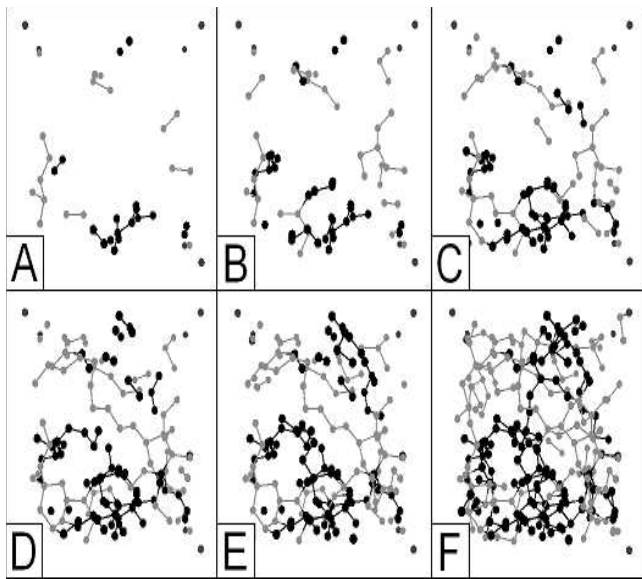


FIG. 2: (A) 1%, (B) 2%, (C) 3%, (D) 4%, (E) 5% and (F) 8% shortest (dark) and longest (light) bonds of model M_1 .

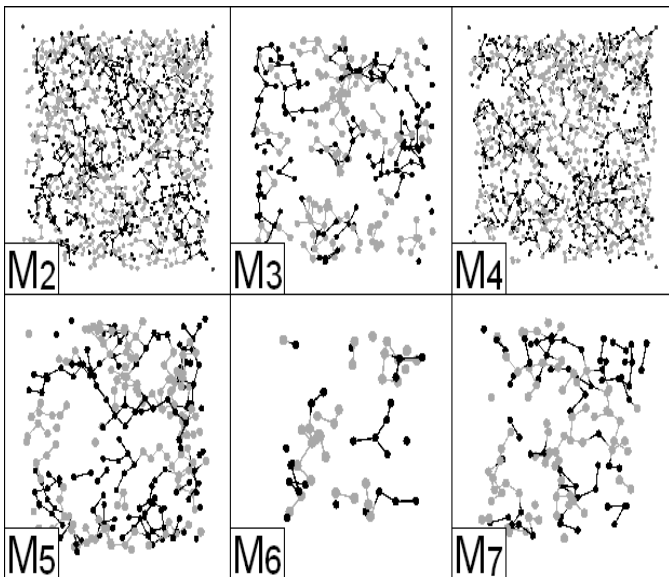


FIG. 3: 4% shortest (dark) and longest (light) bonds of model M_2 , M_3 , M_4 , M_5 , M_6 and M_7 .

firmly that there is a correlation among the same-type-bonds, with a correlation radius around 6.0\AA for model M_1 . The very similar correlation functions between the 4% shortest and the 4% longest bonds of model M_2 - M_7 are plotted in Fig. 5. A substantial correlation between same-type bonds is revealed for all models, with minor

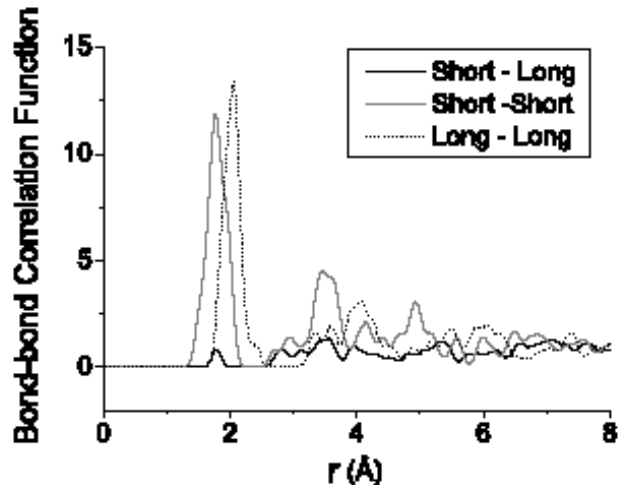


FIG. 4: Bond-bond correlation function between selected bonds of model M_1 . Solid black line denotes pair correlation function between the 4% shortest and the 4% longest bonds. Grey line denotes pair correlation function among the 4% shortest bonds. Dotted line denotes pair correlation function among the 4% longest bonds.

variations from model to model. Model M_1 , M_3 , M_5 and M_6 show slightly stronger effects than the rest. Model M_3 and M_5 show stronger correlations between the short bonds compared to those between the long bonds, while model M_6 and M_7 have relatively stronger correlations between the long bonds than those between the short bonds.

C. Persistence of correlation effects with *ab initio* relaxation

The correlations are found quite consistently in the several models we examined, suggesting that the effects are not modeling artifacts. We also undertook a simple comparison to see how a conjugate gradient (CG) relaxation process by SIESTA affects the models. A relaxation was done on model M_1 and M_9 . While there were slight modifications in structure due to the CG process, we didn't observe any significant changes in these correlations.

D. Persistence of correlation at finite temperature

To further explore the likelihood that the long and short inter bond correlations were artifacts, we also undertook thermal MD simulations at 300K on two small models (M_8 and M_9) with the code SIESTA. Nosé dynamics were used. With some thermally-induced fluctuations, the short-short bond correlation and long-long

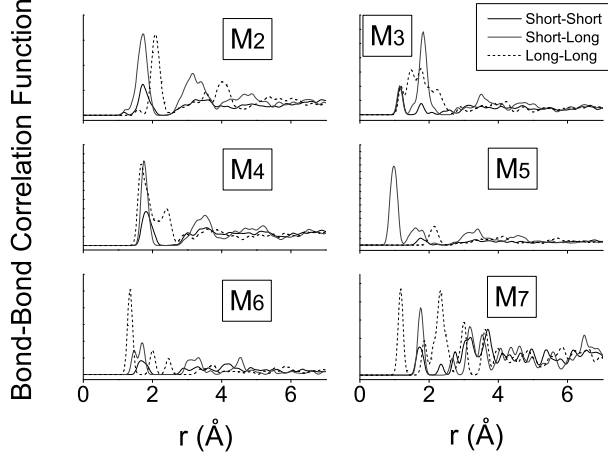


FIG. 5: Bond-bond correlation functions between selected bonds of model M₂, M₃, M₄, M₅, M₆ and M₇. Solid black line denotes pair correlation function between the 4% shortest and the 4% longest bonds. Grey line denotes pair correlation function among the 4% shortest bonds. Dotted line denotes pair correlation function among the 4% longest bonds.

bond correlation persist at all times, as seen in Fig. 6 for model M₉, where the heights of the first peaks of the pair correlation functions from Eq. (1) are plotted throughout time steps. 4% shortest bonds and 4% longest bonds of the system at all time were involved for the calculations. The correlations between the same types of bonds are fluctuating but generally higher than that between the different types. The detailed temperature dependence in this correlation, however, requires further study.

III. ELECTRONIC STRUCTURE

A. Density of states and Localization

The electronic and optical properties of the models are determined by the coordinates of the atoms. Electronic eigenstates and wavefunctions of the models are obtained for static lattices. For the larger model M₂ and M₄ a tight binding model^{22,23} is applied. For other models, the *ab initio* code SIESTA²⁴ is used. Results are very similar for the empirical and *ab initio* calculations.

Densities of states near E_f of the seven models are given in Fig. 7. Spatial localization is reported using the Inverse Participation Ratio (IPR) in Fig. 8. Model M₁ and M₅ are defect free, with no states in their optical gaps. Model M₂ has 0.2% defects and one gap state. Model M₃ and M₄ both have 4% defects, and a small peak of states in the gap. M₆ has 12.5% defects and M₇ has 12% defects and both have many states spread through the gap. Only M₁, M₂ and M₅ conform closely

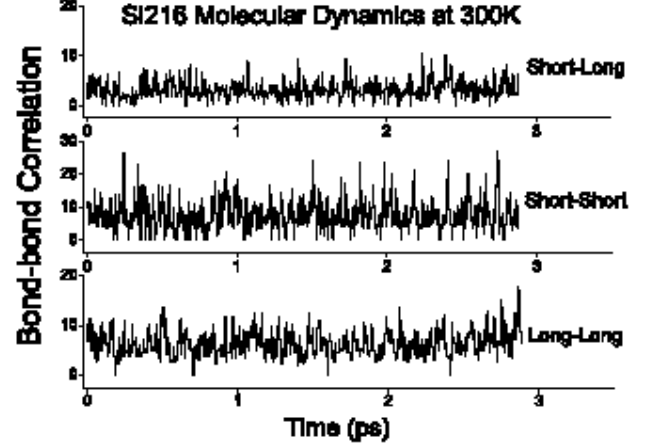


FIG. 6: Correlation (1) between the 4% shortest bonds and the 4% longest bonds; (2) among the 4% shortest bonds; (3) among the 4% longest bonds of model M₉ throughout time steps at 300K. Nosé dynamics were used.

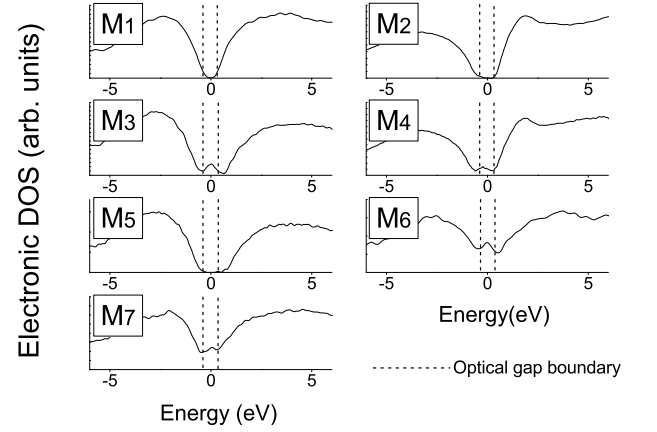


FIG. 7: Densities of states of models. Dashed lines indicate optical gaps. Fermi levels are all shifted to 0.0 eV.

to ordinary expectations for an a-Si DOS. M₃, M₄, M₆ and M₇ exhibit too many defects for good a-Si materials and are studied here mainly for comparison purpose.

B. Topology of band tail states

1. Filamentary structure

The most-localized states of model M₁, displays a 1-D filament connectivity. For state #1024(-0.34eV, a valence state) and State #1025(0.34eV, a conduction state) the

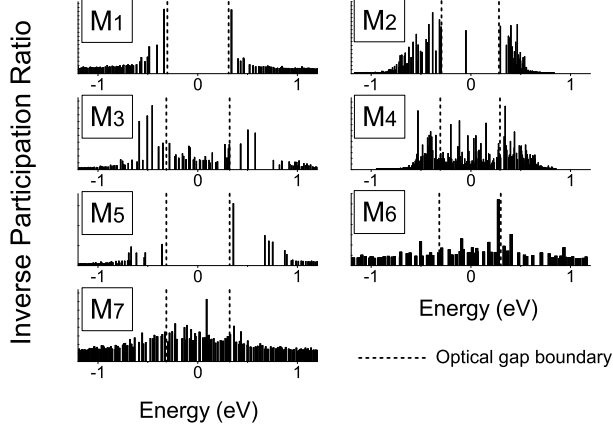


FIG. 8: Spatial localization obtained from IPRs (Inverse Participation Ratio) of models. Dashed lines indicate optical gaps. Fermi levels are all shifted to 0.0 eV. For M_2 and M_4 only a small part of IPRs near the Fermi level is shown.

most electron-probable atoms are selected and shown in Fig. 9. Interestingly, in both case, the atoms locate closely (localization) and happen to form filament (chain) like structures. In addition, the angles along the chain of E#1024 are all small angles, and the bonds are all short bonds. The angles along the chain of E#1025 are all large, and the bonds all long.

Localized states of the other six models, M_2 to M_7 , were also examined. We picked the most localized state for each model. Only the atoms possessing most charge are shown in Fig. 9. We see that, for all these models, these localized atoms form filament-like structures in general. The strength of the effect varies only slightly among the models.

2. Bond length-electron correlations and bond angle-electron correlations near E_f

Fedders, Drabold, Nakhmanson's study¹¹ observed that valence tail states preferentially involved short bond lengths, whereas conduction tail states tended to be involved with longer bond lengths. Angle distortion was also mentioned but no specific relation to the band tails was detected. Related work was undertaken in Ref.¹². Here, we extend this analysis to our collection of models. Where the bond lengths are concerned, the present work is consistent with these findings. In addition we also clearly detect a correlation between valence tail and small bond angle, and a correlation between conduction tail and large bond angle, which has not been explicitly observed before.

An electron(Mulliken charge)-weighted mean bond length for each state was calculated in Ref.¹¹, and it re-

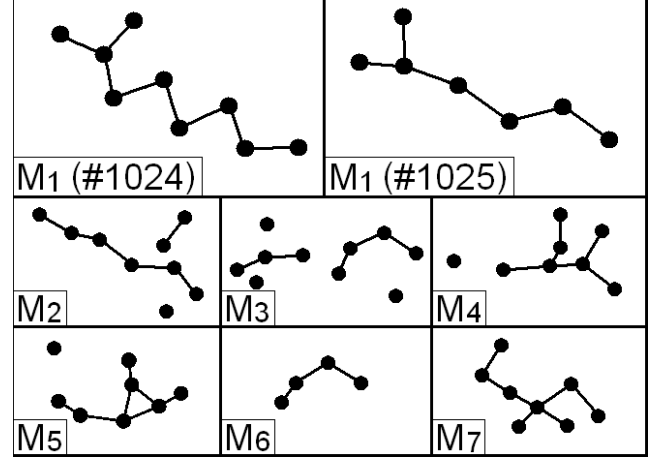


FIG. 9: Most localized electronic eigenstates of model M_1 , M_2 , M_3 , M_4 , M_5 , M_6 and M_7 . Approximately 60% - 75% charge of the state is shown in each case. For model M_1 , both a valence tail state(#1024) and a conduction tail state(#1025) are shown.

vealed an interesting and general trend in bond lengths. Here we computed the mean bond length in a similar fashion, and explored into seven of our models for this mean value. We then extended the calculations into the mean bond angles, using the very same Mulliken charge.

For a certain eigenstate E , the Mulliken charge $q_{(n,E)}$ is the electron probability on an atom n . Using it as a weighting factor, we define the corresponding symmetrized mean bond length as $B_{(E)}$.

$$B_{(E)} = \frac{\sum_{n,m} b_{(n,m)} q_{(n,E)} q_{(m,E)}}{\sum_{n,m} q_{(n,E)} q_{(m,E)}} \quad (2)$$

where n, m summations *only* go over all the possible bonds in a unit cell (of N atoms), with n, m as the bond end atoms. $q_{(n,E)}$, as defined, is the electron probability on the atom n . $B_{(E)}$ (near the Fermi level) for each model is plotted in Fig. 10. $B_{(E)}$ shows an asymmetrical split around the gap (Fermi level) for all models. Smaller average bond lengths are correlated to the valence tails and large average bond lengths correlated to the conduction tails. There are clear difference among the seven models, especially on the mid-gap states from the models with high defect concentration. For models with fewer defect states in the gap, the bond-electron correlations are very clear. Models with many mid-gap states show mixed behavior, though the asymmetric splitting is always detectable.

In analogy with the discussion for bond lengths, we define the electron-weighted mean of bond angles as:

$$A_{(E)} = \frac{\sum_{n,m,l} \theta_{(n,m,l)} q_{(n,E)} q_{(m,E)} q_{(l,E)}}{\sum_{n,m,l} q_{(n,E)} q_{(m,E)} q_{(l,E)}} \quad (3)$$

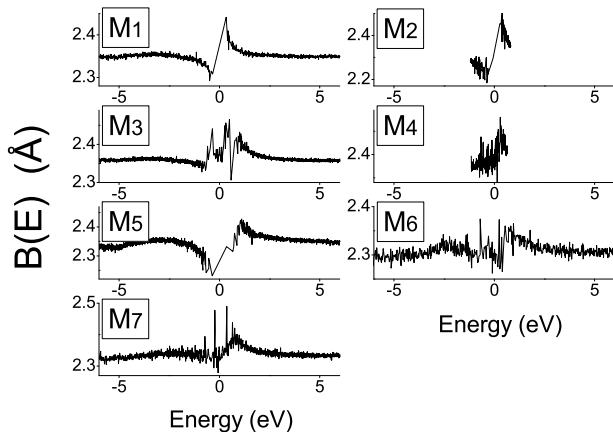


FIG. 10: $B(E)$, the electron-weighted average of bond length near the Fermi levels for the seven models. Only small fractions of data are showing for M_2 and M_4 .

where n, m, l are the atoms of the unit cell of N atoms; summations of n, m, l *only* count over all the possible bond angles, with m as the vertex of each angle. $q_{(n,E)}$, as defined, is the electron probability on the atom n . $A(E)$ is plotted in Fig. 11. It also shows a clear asymmetrical splitting around the gap for all plots. Smaller average bond angles clearly appear to be correlated to the valence tails and larger average bond angles correlated to the conduction tails. There are also differences among the models but the asymmetric feature remains. Interestingly, these angle-electron correlations show strong resemblance to the bond-electron correlations discussed above. It is also natural to connect these correlations to the filamentary structures shown in Fig. 9. For M_1 , which is a typical example, the structure from state #1024 (a valence tail state) has both short bonds and small bond angles along the chain, while #1025 (a conduction tail state) has both long bonds and large bond angles along the chain.

One feature to note is that here only the energies near the Fermi level are shown. In our models, $A(E)$ and $B(E)$ also have extrema in other spectral gaps, whenever the states are fairly localized.

IV. DISCUSSION

Here we offer some heuristic explanation of the last two sections. In a-Si, there are two kinds of random potentials leading to the localization of carriers: point defect (missing atoms or impurities) and topological disorder. The former produces very localized states which lie in the neighborhood of the Fermi level. These are bound states around the point defects, and sit in the middle of gap. The scattering suffered by the carriers is so strong

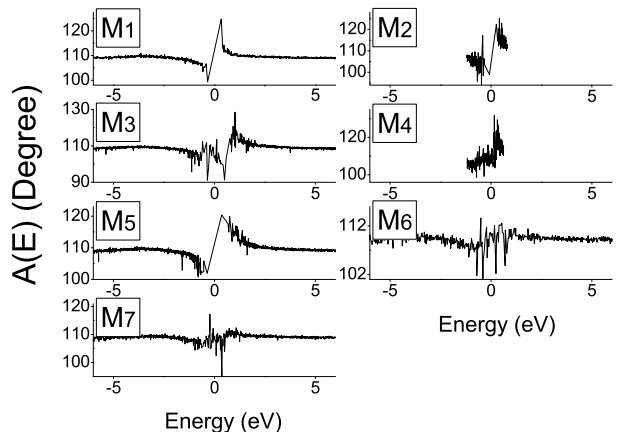


FIG. 11: $A(E)$, the electron-weighted average of bond angle near the Fermi levels for the seven models. Only small fractions of data are showing for M_2 and M_4 .

that the localization length of those states is smaller than the average bond length (for example, the lone electron in dangling bond).²⁵ In contrast, topological disorder, the deviation of bond lengths and bond angles from their crystalline values, produces localized states primarily lying in the tails of the valence band and the conduction band. The localization length of those tail states may extend from one bond length to a range including many atoms depending on the structure of the network.

Band tails exhibit localization because the density of states in their energy range is small, and there is less opportunity for delocalization via mixing, as discussed in the “resonant cluster proliferation” model.^{10,26} In this picture, it is doubtful that an initially localized energy state could persist in the midst of a continuum; it would inevitably mix with the reservoir of resonant states, if there was any overlap between the reservoir and localized state. Similarly, a well-localized state would survive if placed in a region of zero density of states. From this point of view, the band tails are simply between these limits.

According to the scattering theory of solids,^{25,27,28} the distortion of the atomic configuration from crystal mixes Bloch states with different band indices and wave vectors. If these secondary scattering components have large enough phase shifts relative to the primary Bloch wave outside the distorted region, they will interfere destructively, because the phase memory related to the primary Bloch wave has been lost. While inside the distorted region, secondary scattering components are almost in-phase with the primary Bloch wave (phase shift is less than π), and they will interfere constructively inside this region. Thus if a distorted region can produce scattered components with large momentum transfer, a localized state can be formed by the interference of secondary com-

ponents with the primary Bloch wave.

With this mechanism, it is possible that several localized states have peaks in the same distorted regions. This was observed in previous work¹⁰ on M_2 . We explored other models, M_4 and M_7 , and found similar states with overlapping clusters in space. On the other hand, one localized state may have several peaks in structurally distorted regions which are spatially separated (Fig. 9).

The observation that valence tail states are preferentially localized on short bonds and conduction tail states localized on long bonds (Fig. 10) can be understood as follows. Short bond length has two consequences: (1) it will increase the transition integral; the energy of valence band states are lowered while the energy of conduction states is lifted relative to a hypothetical reference crystal (diamond for a-Si); (2) Small bond lengths increase the charge at the center of the bonds (states near valence edge). Thus if we make the significant assumption that the valence and conduction tails should be associated with either short or long bonds, it is clear that the electronic (band-energy) is optimized if the valence tails are associated with short bonds, and the long bonds would “do the least damage” if put above the Fermi-level,

or linked with the conduction tail. This completely neglects other contributions to the total energy, though the observation of the effect in density functional calculations suggests that the band energy *is* the key term.

V. CONCLUSION

We have discovered significant and reasonably model-independent features of the network and electronic structure of a-Si. We believe that the results may prove relevant to a number of other systems as well.^{5,8}

VI. ACKNOWLEDGEMENTS

We thank the Army Research Office under MURI W91NF-06-2-0026, and the National Science Foundation for support under grant No. DMR 0600073, 0605890. We acknowledge helpful conversations with T. Abtew and F. Inam.

-
- * Electronic address: pan@phy.ohiou.edu
† Electronic address: zhang@phy.ohiou.edu
‡ Electronic address: drabold@ohio.edu
- ¹ F. Urbach, Phys. Rev. **92**, (1953) 1324.
 - ² S. Aljishi, J. D. Cohen, S. Jin and L. Key, Phys. Rev. Lett. **64**, (1990) 2811.
 - ³ N. Bacalis, E. N. Economou and M. H. Cohen, Phys. Rev. B **37**, (1987) 2714.
 - ⁴ M. H. Cohen et al, IBM J. Res. Develop. **32**, No. 1 (1988).
 - ⁵ J. C. Phillips, Phys. Rev. B **75** (2007) 214503, and references therein.
 - ⁶ J. C. Phillips, Phil. Mag. B **79** (1999) 527.
 - ⁷ K. McElroy, J. Lee, J. A. Slezak, D.-H. Lee, H. Eisaki, S. Uchida and J. C. Davis, Science **309** (2005) 1048.
 - ⁸ St. Adams and J. Swenson, Phys. Rev. Lett. **84** (2000) 4144.
 - ⁹ S. Maslov and I. Ispolatov, Proc. Nat. Acad. USA **104** (2007) 13655.
 - ¹⁰ J. Dong and D. A. Drabold, Phys. Rev. Lett. **80**, (1998) 1928.
 - ¹¹ P. A. Fedders, D. A. Drabold and S. Nakhmanson, Phys. Rev. **58**, (1998) 15624.
 - ¹² H. C. Kang, Journal of Non-Crystalline Solids **261** (2000) 169-180.
 - ¹³ T. A. Abtew, M. Zhang and D. A. Drabold, Phys. Rev. B **76**, (2007) 045212
 - ¹⁴ R. A. Street, *Hydrogenated amorphous silicon*, Chap 4, Cambridge Univ. Press, Cambridge UK (2002)
 - ¹⁵ F. Wooten, K. Winer and D. Weaire, Phys. Rev. Lett. **54**, (1990) 1392.
 - ¹⁶ N. Mousseau and G. T. Barkema, Phys. Rev. B **61** (2000) 1896.
 - ¹⁷ S. Nakhmanson, P. M. Voyles, N. Mousseau, G. Barkema and D. A. Drabold, Phys. Rev B **63** (2001) 235207.
 - ¹⁸ P. Biswas, R. Atta-Fynn and D. A. Drabold, Phys. Rev. B **69**, (2004) 195207
 - ¹⁹ B. R. Djordjevic, M. F. Thorpe and F. Wooten, Phys. Rev. B **52**, (1995) 5685.
 - ²⁰ N. Bernstein, J. L. Feldman and M. Fornari, Phys. Rev. B **74**, (2006) 205202
 - ²¹ J. Dong and D. A. Drabold, Phys. Rev. B **54**, (1996) 10284.
 - ²² D. Weaire and M. F. Thorpe, Phys. Rev. B **4**, 2508 (1971).
 - ²³ L. Colombo, Computational Material Science **12** (1998) 278.
 - ²⁴ J. M. Soler *et al*, J. Phys: Condens. Matter **14** (2002) 2745.
 - ²⁵ J. Callaway, Quantum theory of the solid state, Chaper 5, New York, Academic Press, (1974).
 - ²⁶ J. J. Ludlam, S. N. Taraskin, S. R. Elliott and D. A. Drabold, Phys. Cond. Matter **17**, (2005) L321.
 - ²⁷ J.M. Ziman, Models of Disorder, Cambridge University Press, (1979).
 - ²⁸ M.L. Goldberg and K.M. Watson, Collision Theory, John Wiley & Sons Inc. (1964).
 - ²⁹ C. Cohen-Tannoudji, J. Dupont-Roc and G. Grynberg, Atom-Photon Interactions, *Basic Processes and Applications*, John Wiley & Sons Inc. (1998).